Spatial distribution of PXR generated by 855 MeV electrons: comparison of simulation results with experimental data

Goponov Yu.A.[a], Sidnin M.A.[a], Vnukov I.E.[a], Behrens C.[b], Kube G.[b], Lauth W.[c], Gogolev A.S.[d]*, Potylitsyn A.P.[d]

[a]*Belgorod National Research University, Belgorod, Russia*
[b] *DESY, 85 Notkestra , 22607 Hamburg, Germany*
[c] *Institut fur Kernphysik, 45 Johann-Joachim-Becher-Weg, 55128 Mainz, Germany*
[d]*National Research Tomsk Polytechnic University, Tomsk, Russia*

Abstract

The detailed data treatment of the experiment performed in MAMI-B microtron with the X-ray camera, taking into account the contribution of both diffracted transition radiation and bremsstrahlung, is presented. The X-ray camera efficiency was additionally considered. The simulated emission pattern in general agrees with the experimental one. However, along the Bragg direction where the influence of the beam size on the emission spatial distribution is most noticeable, a discrepancy between the model and the experiment is observed. Possible reasons of such discrepancy are discussed.

Keywords: beam diagnostics, parametric X-ray radiation, accelerator, crystal;

1. Introduction

Invasive [1] and noninvasive [2, 3] methods for estimation of the transverse beam size based on registration of optical radiation from metal foils set in the accelerator can't ensure measurement of the beam parameters with sizes about some tens of nanometers because of coherent effects in the radiation [4]. Microbunching instabilities in high-brightness electron beams of modern linac-driven free-electron lasers (FELs) can lead to coherence effects in the emission, thus making it impossible to obtain a direct image of the particle beam, especially for transverse beam profiles. To allow beam profile measurements for small beam size and in the presence of microbunching instabilities, different monitor concepts are considered.

Parametric X-ray radiation (PXR) in thin crystals can be used for this purpose [5, 6]. PXR is emitted when a relativistic charged particle beam crosses a crystal, and the radiation process can be understood as diffraction of the virtual photon field associated with the particles at the crystallographic planes.

Studies on the influence of the electron beam size on the PXR spatial distribution from electrons with an energy of 855 MeV in the silicon crystal thickness of 50 μm using a high-resolution X-ray camera [7] (HRC) based on a thin scintillator coupled waveguides with CCD matrix in experiment [8] confirmed the possibility of estimation of the electron beam size with the help of such measurements.

Using PXR or any other mechanism of radiation to determine the size of an electron beam is possible if we have a good agreement between measured and calculate angular distribution for a point such as an electron beam spot.

Results by already cited work [8] are not described by PXR kinematic theory. At the distribution centre, where the influence of beam size on the radiation spatial distribution is most noticeable, a large difference between the experimental result and kinematic theory prediction was observed [8]. A gap in the centre of the PXR angular distribution which was predicted by PXR theory and usually observed for thin crystals, see, for example [6, 9], occurred very small.

Considering the real photon diffraction for the [8] experiment, an improved correlation between the experimental

* Corresponding author. Tel.: +7 906 954 1950; fax: +7 382 270 5691.
E-mail address: gogolev@tpu.ru.

and calculated data was obtained for the centre of PXR reflex [9]. However, the difference between the experimental and calculation results remains relatively large. Based on what is mentioned above, it is important and relevant to compare the experimental results [8] with calculation taking into account the influence of all experimental conditions more carefully than it was made in Ref. [9] and try to find the reason of the discrepancies observed.

2. Calculation

In the general case in the experiment, all the mechanisms of radiation generation at the Bragg angles are implemented simultaneously; therefore, in comparing experimental results with calculated ones, it is necessary to consider all types of radiation. The kinematic PXR theory describes the results of measurements quite well [10], therefore, the PXR yield was calculated using a PXR spectral-angular distribution formula obtained in the kinematic approximation [11].

For high-energy electrons, the radiation in the X-ray range of photon energy ($\omega \leq 100$ keV) in crystals, except PXR, is generated through the mechanism of the diffracted transition radiation (DTR) and the diffracted bremsstrahlung (DB). The methods of the PXR, DTR, and DB yields calculation, taking into account the electron beam divergence and multiple scattering in the crystal, the emission collimation angle and other experimental conditions are described in detail by Laktionova et. al [9].

The main purpose of this study is to explain the results of the experiment [8], where the PXR kinematic theory does not describe the measurements results without considering the contribution of real photon diffraction and accurate inclusion of the experimental technique characteristics. To analyse the influence of the diffracted real photon contribution and experimental conditions on the angular distribution of the resulting radiation, a series of calculations of radiation yield for the experimental conditions [8] and the (004) reflection order were performed with procedure [9].

The rectangular detector, the size of which is 77.28 × 80.04 μm^2, is moving down through the centre of reflex vertically with a step of 77.28 μm, which corresponds to the angular distribution measurement using an X-ray camera with a pixel size of 11.2 × 11.6 μm^2 for angular capture 3 × 3 pixel and relation between CCD size and the camera field of view ≈ 2.3 [7] (see the next section).

Figure 1a shows the vertical spatial distributions of PXR, DTR, and DB for the first-order reflection calculated by a technique [9], so these are curves 1–3, respectively. Curve 4 is the distribution for all emission mechanisms PXR+DTR+DB. From the figure, it is seen that PXR has a bigger intensity than DB and DTR, and its angular distribution is broader. In the centre of PXR angular distribution, there is a broad failure, whereas the output of DTR and DB is concentrated near Bragg's direction. Thus, the diffracted photon yield gives the main contribution into the radiation yield in the reflex centre. As can be seen from the figure, DTR spatial distribution has a failure in the centre too. However, it is narrower than that of PXR; therefore, spatial distribution of the total radiation yield possesses a narrower minimum than PXR one. The energy of photons of the first allowed reflection order is ω = 23.4 keV < $\gamma\omega_p \approx 50$ keV, which is why the yield of diffracted Bremsstrahlung is suppressed because of the Ter-Mikaelian effect of density [12] and appears to be less than the DTR yield.

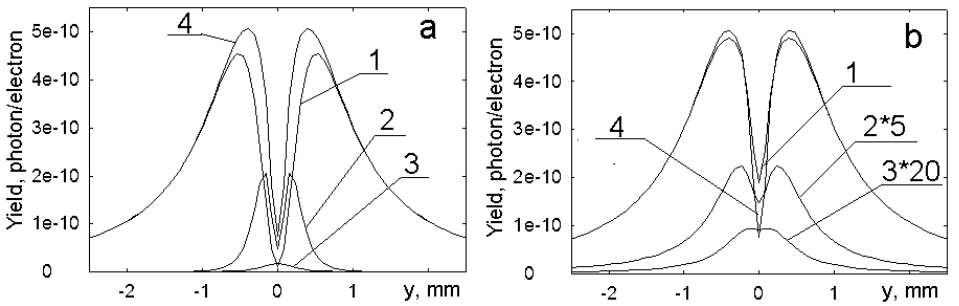

Fig. 1. Spatial distribution of X-ray intensity for (100) reflection plane and the first reflection order in vertical direction (fig. 1a) and total radiation for three reflection order (fig. 1b) for the experimental condition of [8]

As it was remarked in [9], HRC measures the combined angular distribution for all reflection orders rather than for individual orders. Figure 1b shows the vertical spatial distribution of total radiation PXR+DTR+DB for three orders of reflection calculated by a technique [9], considering the spatial size of the electron beam on the crystal, so these are curves 1–3, respectively. It is supposed that the beam spatial distribution is Gauss one with $\sigma_x = \sigma_y = 50$ μm. Curve 4 is the first-order total radiation spatial distribution calculated for a point such as the electron beam.

From the figure, it is seen that the first-order reflection has maximum intensity. The contributions of the second and particularly the third and subsequent orders with higher-energy photons and narrower angular distributions are substantially less. However, the second-order contribution is still significant, and with the help of an absorber in the photon beam between the crystal and the detector, as in the analysed experiment [8], can be comparable with the contribution of the first-order reflection. It should be remarked that following reflection orders have spatial distributions with less depth than the first one. From comparison between calculation results with and without influence of spatial beam size (curve 1 and curve 4 respectively), it is seen that it is concentrated in the distribution centre and decreases the depth of the failure for the first reflection order in approximately 1.5 times.

3. Experimental setup

The analysed experiment [8] was performed at the 855 MeV beam of the Mainz Microtron MAMI (University of Mainz, Germany) in the beamline of the X1 collaboration. Figure 2 shows a sketch of the experimental setup. The beam was operated with a mean beam current of about 0.5 μA and divergence of about 0.1 mrad. The target consisting of a 50 μm thick (100) cut silicon crystal was mounted onto a motorised stage which allowed a precise alignment of the crystallographic planes with respect to the beam axis. In the experiment, the crystal was aligned in Laue geometry in two orientations for the observation of the (220) and the (400) reflex family. A detector was placed under the observation angle of $\Theta_D = 22.5°$, which corresponds to the first-order PXR photon energies of $\omega_{220} = 16.55$ keV and $\omega_{400} = 23.40$ keV, respectively.

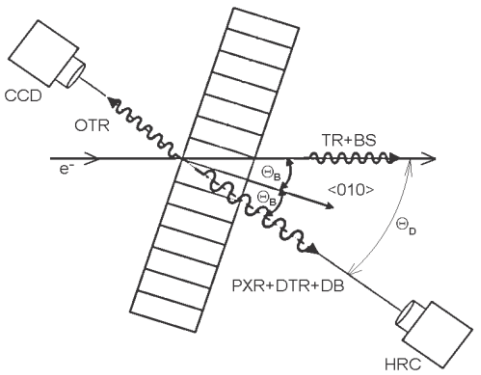

Fig. 2. Sketch of the experimental setup

The distance between the target and the detector is about 350 mm. A compact high-resolution X-ray camera was used as the detector (ProxiVision HR25 X-Ray). It is based on a conventional analogue camera (Sony XC-ST70CE) with a P43 phosphor coating and fibre optics taper in front of the CCD chip with a pixel size of 11.6 × 11.2 μm^2 in horizontal and vertical direction, respectively [7]. Considering the relation between the CCD size of 8.72 × 6.52 mm^2 and the camera field of view 20 × 15 mm^2 [7], we may suppose that its spatial resolution is about 26 μm.

A second CCD detector, mounted in backward direction under an angle of 22.5°, allowed to perform measurements based on optical transition radiation (OTR) which was generated at the entrance side of the crystal, thus allowing to record OTR beam profiles under the same experimental conditions. Measurements of the PXR angular distribution were performed for six different beam configurations with horizontal (1 σ) beam sizes between 45 μm and 260 μm and vertical sizes between 45 μm and 800 μm.

4. Simulation of HRC characteristics

As noted above, in the experiment reported in [8] measurements of radiation angular distributions were carried out by means of the ProxiVision HR25 X-ray camera with a phosphor P43 with composition Gd_2O_2S:Tb and thickness of 30 μm [7]. An entrance aluminium window 0.5 mm thick is placed in front of the phosphorus. In accordance with reference literature, see, e.g., [13, 14] the density of P43 is equal to 7.32 g/cm^3 for solid material. However, in the device, P43 is fixed together with binding material onto the substrate with a packing ratio of about 0.6. That reduces the real phosphor density up to ~4.32 g/cm^3.

Really, this device wasn't measured as an angular distribution of a photon beam but as a response of a detector on

the energy of radiation incoming. It registers the light output in different points of a thin scintillating plate when hit by an X-ray beam. Therefore, to compare the results of calculations of the X-ray radiation yield in thin crystals with measurement results using HRC, simulations of the HRC response to the photon energy of the detected radiation were performed using the Monte-Carlo method. In the simulations, the interaction cross sections for photons with matter were used [15], with values at intermediate photon energies determined by linear interpolation. Photons with fixed energy ω in the range 10 to 100 keV hit the HRC perpendicular to its surface were simulated. These conditions are close to the experimental ones reported in [8] since the distance between the crystal and the detector of l = 350 mm is larger than the typical size of the radiation spot on the detector (~10 mm).

The contribution of scattering processes is more than 1% only for photon energies of ω > 40 keV, where the efficiency of the device is reduced to ~20% from the maximum value (see figure 3), and hence, the contribution of these processes to the response function of the HRC was not considered.

The simulated dependence of the HRC efficiency and the average energy transmitted to secondary electrons (HRC response) on the photon energy received is shown in figure 3 as curves 1 and 2, respectively.

The HRC efficiency in the first approximation may be presented as $\varepsilon(\omega) = \exp(-\mu_{Al}(\omega)\, t_{Al})(1-\exp(-\mu_{phosph}(\omega)\, t_{phosph})$, where μ are absorption linear coefficients of emission energy of ω in these materials. The first term is increased with the increase of photon energy and the second one is decreased. As a result, the HRC efficiency in the low-energy region, where the first reflection order of radiation is observed, is the curve with a maximum for ω ~ 18 keV. Therefore, the detector efficiencies for both crystal orientation and the first reflection order occur approximately the same, (220) ≈ 24% and (400) ≈ 20%, respectively.

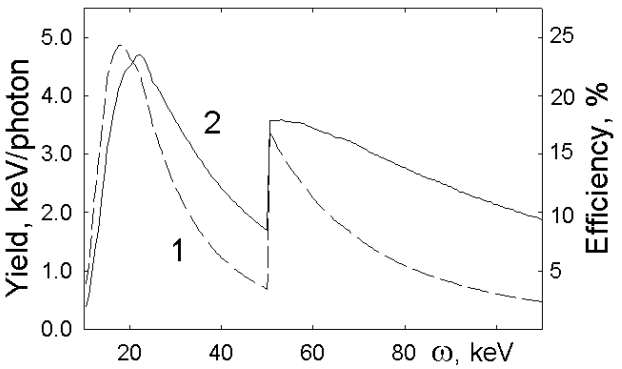

Fig. 3. Dependence of the HRC characteristics on the photon energy

Because of this, for the (400) reflection order, the photon energy is higher than for the (220) one energy transmitted secondary electrons, and the detected response for this crystal orientation is higher also. These values are about 4.56 keV/photon and 3.74 keV/photon, respectively.

5. Measurements results and comparison to the calculations

As mentioned above, measurements were performed for six values of electron beam size and two diffraction planes. For each measurement, 100 beam images with frequency of 25 Hz were taken together with background images. A median filter was applied to remove the pepper noise originating from high energetic background interaction in a single pixel. After this, correction data from all CCD pixels were subdivided on individual spatial distribution in vertical and horizontal directions. Each distribution points include matrix 3 × 3 pixels and have a size of 77.28 × 80.04 μm^2 in vertical and horizontal direction, respectively. It allowed to find the centre of the reflection spot for each crystal orientation and the electron beam configuration. The same procedure was made for background measurements and after that, it was subtracted from the measured distributions.

Results of this procedure for the (400) and (220) reflection families are shown in figure 4 and figure 5 for horizontal and vertical direction points. Measurements were done for the electron beam size (1 σ) of 50 μm in both directions. To estimate the statistical error of the results obtained, we used the rms deviation of the readings of each pixel from the mean value for matrix 3 × 3 pixels. The calculated spatial distributions are shown on the figures by curve. Calculation was made for the same sizes of the detector and electron beam. The calculation results include contribution of three orders of reflection and consider the dependence of the HRC efficiency and response from the photon energy (see figure 3). Because of the HRC absolute sensitivity is unknown correlation between the calculated results and measured ones was made by means of scale coefficient for relatively large distance from the reflection spot centre.

From the figures, it is seen that for a relatively large distance from the reflection centre, agreement between the calculation results and measured ones is comparatively well. However, for the reflex centres, the difference between

the experiment and calculation remains rather large.

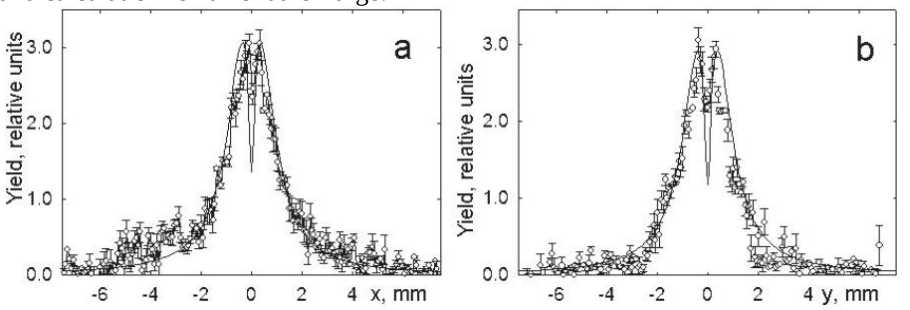

Fig. 4. Spatial distribution of X-ray intensity for (100) reflection plane in horizontal (fig. 4a) and vertical direction (fig. 4b)

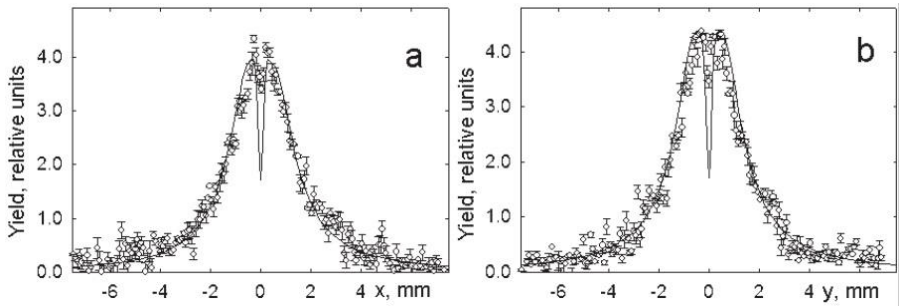

Fig. 5. Spatial distribution of X-ray intensity for (110) reflection plane in horizontal (fig. 5a) and vertical direction (fig. 5b)

The failure depth in the measured distributions is twice less than that in the calculated ones. Moreover, the measured dependence top is narrower than the calculated ones. It is necessary to remark that the scale coefficient for the (110) reflection plane and the (100) one occurs different. For the (400) reflection family, it is 1.4 times higher than for the (220) ones. It means that for the (400) reflection family, the relative measured yield is the same number of times higher. Difference between calculation results for these orientation is about twice, whereas for the experiment it is about 1.3 (see figure 4 and figure 5). It is likely that it is coming from HRC characteristics which were taken for calculation. Presence of more heavy elements in the entrance window or enlarging of the packing ratio increases the HRC efficiency for hard photons and the soft photon absorption. It may enlarge contribution of higher reflection orders with more narrow spatial distribution and decrease the failure.

For the large spatial beam size, the difference between the measurement and calculation results is less. Figure 6 presented measured and calculated results for electron beam sizes are 44.7 μm and 796 μm in horizontal and vertical directions for the (220) reflection family.

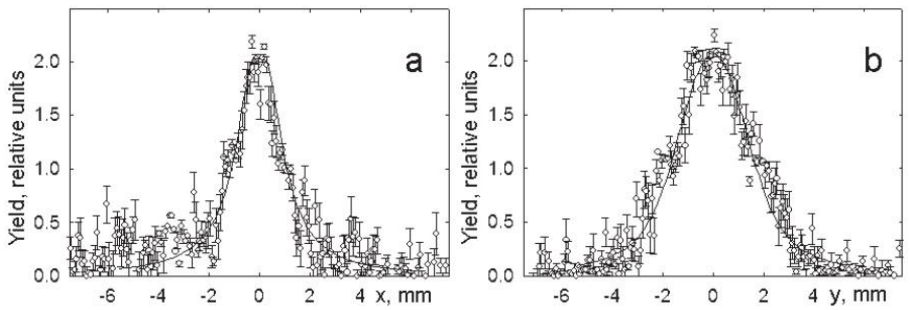

Fig. 6. Spatial distribution of X-ray intensity for (110) reflection plane in horizontal (fig. 6a) and vertical direction (fig. 6b)

From the figures, it is seen that agreement between the calculation and measurements is better especially for the

vertical direction where the beam size influence on the measured distribution is dominated. However, for the large beam size also, the scale coefficient for the (400) reflection family is greater than for the (220) one. For the horizontal distribution, experimental points on the distribution maximum are placed inside the calculated curve.

6. Summary

The results of the present research could be briefly stated as follows: (1) The method of electron beam size estimation by means of photon emission in thin crystal measurements with X-ray a coordinate sensitive detector proposed in [5] may be used when the spatial size of measured emission is comparable with the beam size investigated; (2) PXR theory explains results of the paper [8] for large observation angles rather well. Considering real photon diffraction contribution improves the agreement between the experimental and calculation. Difference for small observation angles may be explained by the characteristics of the X-ray camera.

Acknowledgements

The work was supported by the Ministry of Education and Science of the Russian Federation grant № 3.1903.2017 and the Russian Science Foundation (Project N 15-12-10019).

References

1. Fiorito R.B. 2009 Proc. PAC'09 (Vancouver) TU3GRI02.
2. Urakawa J. et al 2001 Nucl. Instrum. Methods A 472 309.
3. Kube G., Backe H., Lauth W. and Schope H. 2003 Proc. DIPAC2003 (Mainz) IT09.
4. Loos H., Akre R., Decker F.-J. et al 2008 Proc. FEL08 (Gyeongju) THBAU01.
5. Gogolev A., Potylitsyn A. and Kube G. 2012 J. Phys. Conf. Ser. 357 012018.
6. Takabayashi Y 2012 Phys. Lett. A 376 2408.
7. High-Resolution X-Ray Camera, http:www.proxivision.de/datasheets/X-Ray-Camera-HR25-x-ray-PR-0055E-03.pdf.
8. Kube G., Behrens C., Gogolev A.S. et al 2013 Proc. IPAC2013 (Shanghai) MOPMEO11.
9. Laktionova S.A., Pligina O.O., Sidnin M.A. and Vnukov I.E. 2014 J. Phys. Conf. Ser. 517 012020.
10. Brenzinger K.-H., Limburg B., Backe H. et al 1997 Phys. Rev. Lett. 79 2462.
11. Nitta H. 1991 Phys. Lett. A 158 270.
12. Ter-Mikaelian M.L. 1972 High-Energy Electromagnetic Processes in Condensed Media (New York: Wiley Interscience).
13. Uesugi K., Hoshino M. and Yagi N. 2011 J. Synchrotron radiation 18 217.
14. High-Resolution X-Ray Camera, http://www.proxivision.de/datasheets/X-Ray-Camera-HR75-x-ray-PR-0038E-03.pdf.
15. Berger M.J. and Hubbell J.H. http://www.nist.gov/pml/data/xcom/index.cfm (data 12/10/2015).